MRS Communications (2014), *4*, 183–188
© Materials Research Society, 2014
doi:10.1557/mrc.2014.33

MRS Communications

Research Letters

Significant α-phase growth confinement in Grade 4 titanium and substantial β-phase refinement in Grade 7 titanium

M. Yan, M. Qian, and **T.T. Song,** RMIT University, School of Aerospace, Mechanical and Manufacturing Engineering, Centre for Additive Manufacture, Melbourne, Victoria 3001, Australia
M. Yan and **M.S. Dargusch,** Queensland Centre for Advanced Materials Processing and Manufacturing, The University of Queensland, Brisbane, Queensland 4072, Australia
X.S. Wei, Department of Mechanical Engineering, University of Melbourne, Melbourne, Victoria 3010, Australia
Address all correspondence to M. Qian, M.S. Dargusch at **ma.qian@rmit.edu.au; m.dargusch@uq.edu.au**

(Received 28 August 2014; accepted 12 November 2014)

Abstract

Significant α-phase growth confinement in Grade 4 titanium (Ti) and substantial β-phase refinement in Grade 7 Ti were observed during high-temperature annealing. The mechanism for each observation was identified through detailed microstructural investigation assisted with phase diagram analyses. The former observation was due to the pinning effect of Fe-stabilized grain boundary (GB) β-Ti phases in Grade 4 Ti. The latter observation resulted from the redistribution of Fe and, palladium (Pd) in particular, in Fe-stabilized and Pd-containing GB β-Ti phases in Grade 7 Ti. Pd was found to exist mainly in two forms in cold-rolled Grade 7 Ti, i.e. Fe-stabilized GB β-Ti phases and an occasionally observed orthorhombic $Ti_{88}Pd_9Fe_3$ phase. The latter is close to the Ti_2Pd_3 intermetallic phase in terms of the crystal structure.

Introduction

Unalloyed titanium (Ti) is normally referred to as commercially pure (CP) Ti which contains a small amount of interstitial elements.[1–3] CP-Ti has four grades, Grades 1–4. They have excellent ductility, specific strength, and biocompatibility, used in a variety of industries such as chemical processing, biomedical, aerospace, and offshore drilling. Grade 7 Ti alloy is a variant of CP-Ti mildly alloyed with palladium (Pd; 0.12–0.25 wt.%) for improved resistance to corrosion, especially in oxidizing Cl^- solutions.[4] A similar alloying element for Ti is ruthenium (Ru), which is introduced to CP-Ti in the range of 0.08–0.14 wt.%[5] and to biomedical β-Ti alloys up to 2.6 wt.%.[6] Altogether CP-Ti and Grade 7 Ti products account for ~25% of the overall Ti market, and they continue to draw much attention from a research perspective.[7–9]

Both oxygen and iron are common impurities in CP-Ti and Grade 7 Ti with different specifications.[1–3] As for Fe, Grades 4 and 7 Ti are allowed to contain up to 0.5 wt.% Fe and 0.3 wt.% Fe, respectively.[10] Fe is a potent β stabilizer and therefore is an important alloying element for designing high-strength Ti alloys.[11,12] It can noticeably affect the microstructure of CP-Ti materials even at a trace level, e.g., 1280 ppm.[8,13] Regarding the Grade 7 Ti, although its superior resistance to corrosion in Cl^--containing environments has been well established, the existing form of Pd in the alloy remains controversial, with claims of Pd being present in Pd–O surface oxides[1] or being associated with β-Ti.[14]

In the present study, both as-received (cold-rolled) and heat-treated Grade 4 CP-Ti and Grade 7 Ti have been investigated in detail, using Grade 1 Ti as a point of reference. Heat treatment of cold-rolled Ti materials can enhance ductility to achieve desired strength–ductility combinations.[15–18] It was found that after annealing at 1000 °C, Grade 1 CP-Ti showed evident grain growth in its α phase but unusual phenomena were observed in Grade 4 CP-Ti and Grade 7 Ti: (a) significant α-phase growth confinement occurred in Grade 4 CP-Ti and (b) substantial β-phase refinement occurred in Grade 7 Ti, when compared with the microstructures prior to annealing. The mechanisms for each observation were identified through comprehensive microstructural studies and phase diagram analyses. In addition, the existing form of Pd in the Grade 7 Ti alloy was determined.

Experimental

The chemical compositions (Fe, Pd, and O) of the cold-rolled bars of Grades 1, 4, and 7 Ti are listed in Table I, satisfying

Table I. Compositions of the Ti materials studied (Grades 1, 4, and 7). Impurity levels of other elements such as N and C are not listed.

Composition (wt.%)	Grade 1	Grade 4	Grade 7
Fe	0.2	0.5	0.3
Pd	–	–	0.2
O	0.18	0.4	0.25
Ti	99.5	99.0	99.0

https://doi.org/10.1557/mrc.2014.33 Published online by Cambridge University Press

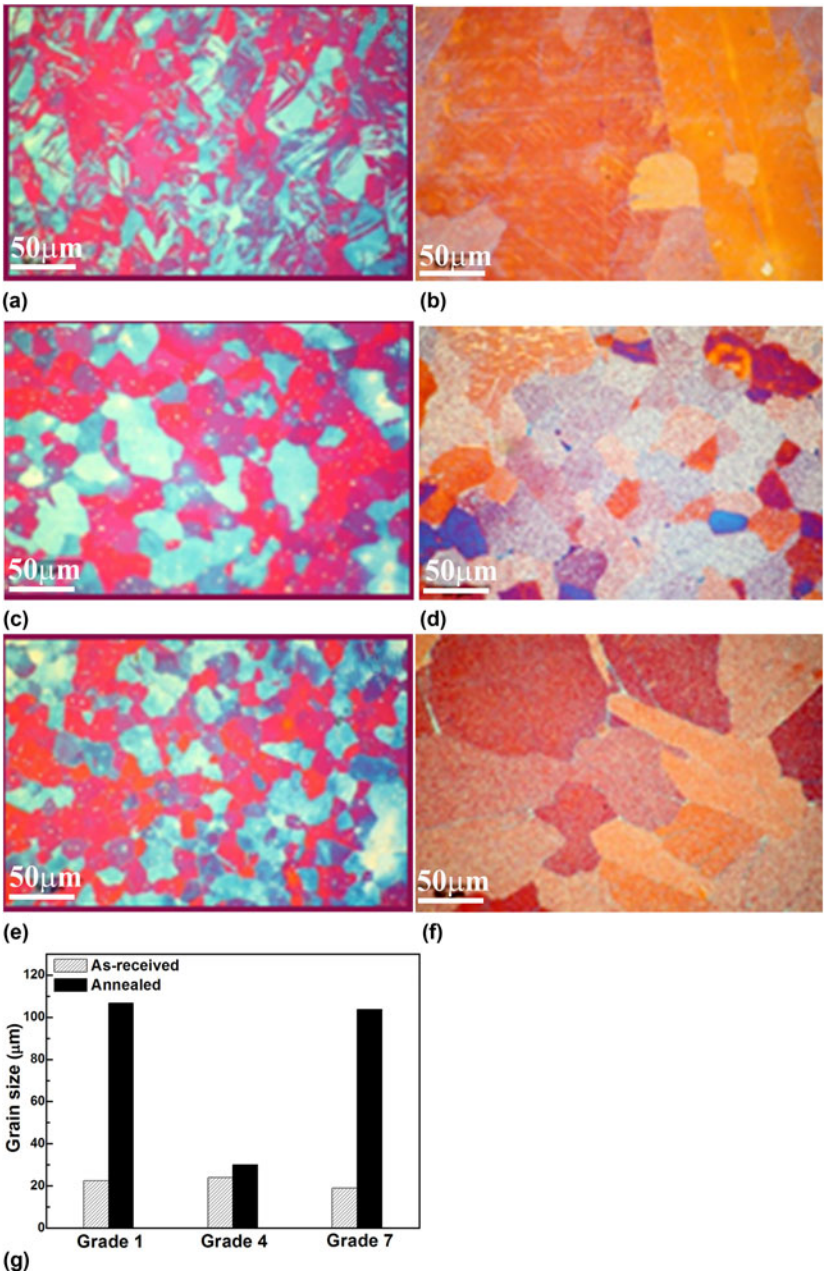


Figure 1. Optical microstructures of the as-received (cold-rolled) and as-annealed CP-Ti materials: (a) and (b) for Grade 1, (c) and (d) for Grade 4, (e) and (f) for Grade 7. The as-annealed CP-Ti shows evident α phase growth except Grade 4. (g) summarizes the average grain size of the α-Ti phase in these CP-Ti materials.

respective ASTM specifications. Samples of each Ti material was annealed in a differential scanning calorimeter (DSC; Netzsch) at 1000 °C for 30 min in a high-purity argon flow (20 ml/min), followed by furnace cooling (cooling rate was ~10 °C/min).

The microstructures of the as-received (cold-rolled) and as-annealed samples were analyzed using optical microscopy (OP; Leica), scanning electron microscopy (SEM; JEOL 7001), and transmission electron microscopy (TEM; Philips Gatan F20, 200 kV). A focused ion beam (FIB; XT Nova Nanolab 200) using a Ga source was used to prepare TEM samples. The beam current was applied in a step-down fashion to progressively remove any damaged layer from previous operations and to minimize beam damage.[19] The composition was analyzed using energy-dispersive x-ray spectroscopy [EDX; Si (Li) detector; standardless] attached to the TEM. The average grain size of each sample was determined from measuring 200 grains.

https://doi.org/10.1557/mrc.2014.33 Published online by Cambridge University Press

Results

Figures 1(a) to 1(f) compare the microstructural differences between the cold-rolled and as-annealed Grades 1, 4, and 7 Ti. Fig. 1(g) summarizes the average grain size of each material. The results show that:

- The grain size of the as-annealed Grade 1 increased markedly after annealing at 1000 °C [see Figs. 1(a), 1(b), and 1(g)]. The same observation occurred to the α-Ti phase in the as-annealed Grade 7 Ti as well [Figs. 1(e), 1(f), and 1(g)].
- In contrast, there was significant α-Ti phase growth confinement in the as-annealed Grade 4 CP-Ti whose grain size (of α-Ti phase) remained almost the same as the cold-rolled material [Figs. 1(c), 1(d), and 1(g)].

Figure 2(a) reveals that there are extensive secondary phases existing in the grain boundary (GB) areas of the cold-rolled Grade 4 CP-Ti. These secondary phases may have inhabited GB movement serving as the underlying reason for the grain growth confinement observed in the as-annealed Grade 4 CP-Ti. They were identified as Fe-stabilized β-Ti phases. A typical TEM SAED of this phase is shown in Fig. 2(b) along with a TEM SAED pattern from the α-Ti matrix [Fig. 2(c)]. TEM–EDX results exploring the phase constitution are shown in Fig. 3(f).

Fe-stabilized GB β-Ti phases were also observed in the cold-rolled Grade 7 Ti alloy. Figures 2(d) and 2(e) present a TEM bright-field image of one such Fe-stabilized β-Ti phase and the corresponding SAED pattern, respectively. TEM–EDX results suggest that the phase contained Pd in the range of about (2–4 at.%). Electron diffractions of another type of Pd-containing phase (~$Ti_{88}Pd_9Fe_3$ in at.% as measured by TEM–EDX), observed only occasionally in the cold-rolled microstructure, are presented in Figs. 2(f) and 2(i). These SAED patterns suggest that this $Ti_{88}Pd_9Fe_3$ phase has a relatively large lattice parameter along its b-axis and appears to be an orthorhombic phase with $a \approx 3.7$ Å, $b \approx 15.0$ Å, and $c \approx 5.2$ Å, making it close to the Ti_2Pd_3 intermetallic phase in terms of the crystal structure.[20–22] These two Pd-containing phases are, however, different in phase constitution. Ti_2Pd_3 is an uncommon phase at room temperature according to the Ti-rich Ti–Pd binary phase diagram [see Fig. 4(a)[23]].

Aside from the significant grain growth confinement observed in the Grade 4 CP-Ti, another notable feature observed from the as-annealed microstructures of Grades 4 and 7 Ti is the much reduced grain size of the β-Ti phase in the Grade 7 Ti. Figure 3 compares the microstructures of the Grade 7 Ti before [Fig. 3(a)] and after annealing [Fig. 3(b)]. The tens of micrometers long, Fe-stabilized β-Ti phases (up to ~40 μm) are reduced to (1–2 μm) round particles. Figure 3(c) presents a TEM bright-field image of one such β-Ti phase particle. The surrounding matrix remains to be α-Ti, Fig. 3(d). The β-Ti phase retains its crystal structure after annealing, with typical SAED patterns

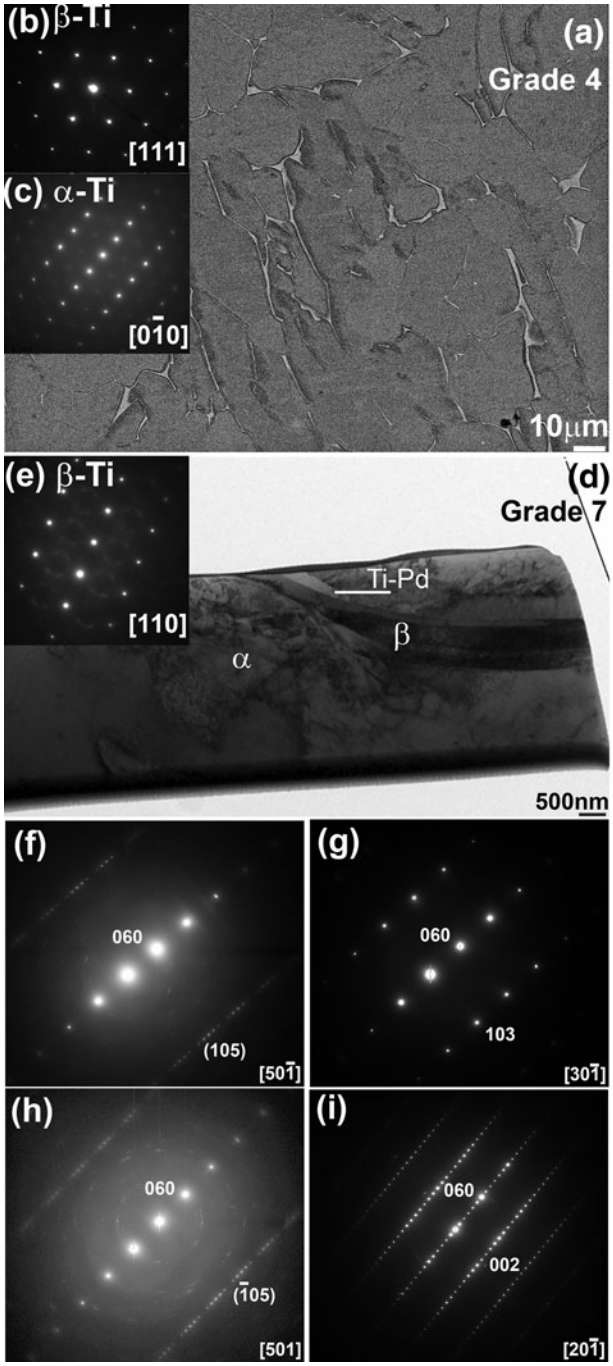


Figure 2. (a) SEM–BSE image showing the Fe-stabilized β phase in the GB area of the as-received (cold-rolled) Grade 4 CP-Ti, (b) TEM–SAED patterns from an Fe-stabilized β phase, (c) TEM–SAED pattern from an α-Ti phase, (d) TEM bright-field image and (e) corresponding SAED pattern for the Fe-stabilized β phase in the as-received (cold-rolled) Grade 7 Ti, and (f) SAED patterns of the orthorhombic phase ($Ti_{88}Pd_9Fe_3$ in at.%) occasionally observed in the cold-rolled Grade 7 Ti.

shown in Fig. 3(e). The additional diffraction features in the SAED patterns in Fig. 3(e) are associated with the ω phase.[8,24]

Figure 3(f) summarizes the TEM–EDX results of the β phases (annealed and cold-rolled) and the α phase (annealed)

https://doi.org/10.1557/mrc.2014.33 Published online by Cambridge University Press

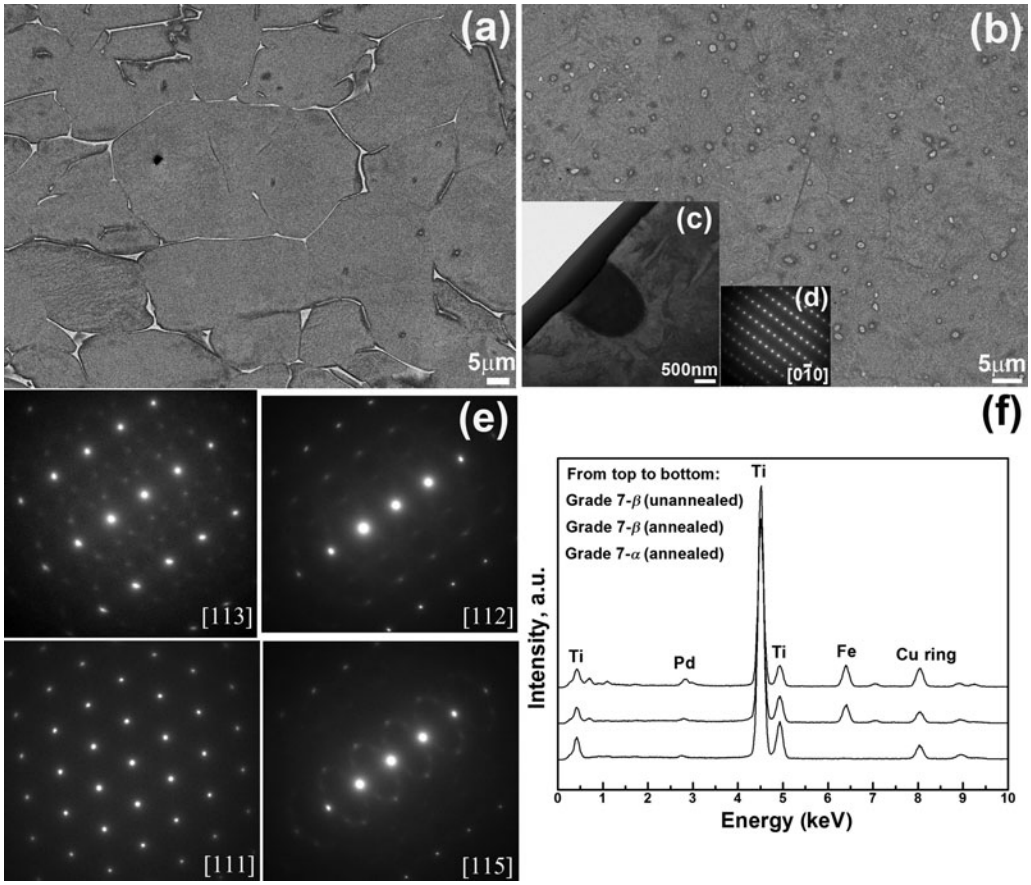


Figure 3. SEM–BSE images comparing the β phase in the (a) as-received (cold-rolled) and (b) as-annealed Grade 7 Ti, (c) a TEM bright-field image for the β-Ti phase particle, (d) an SAED pattern for the surrounding α-Ti grain, (e) a series of SAED patterns for the β-Ti phase in the as-annealed Grade 7 Ti, and (f) comparison of the TEM–EDX results indicating a lowered concentration of both Pd and Fe in the as-annealed Grade 7 Ti.

in the Grade 7 Ti alloy. The β phase prior to annealing contained a high amount of both Pd (~4 at.%), and Fe (~12 at.%), while after annealing a decrease in the concentration of both Pd (down to ~0.6 at.%) and Fe (down to ~8.0 wt.%) was detected, implying solute redistribution of Pd and Fe away from the β-Ti phase during annealing. This is confirmed by the observation that a small amount of Pd was detectable in the surrounding α-Ti matrix (~0.1 at.%) in the as-annealed Grade 7 Ti, while no Pd was detected prior to annealing. As will be shown below, this is the reason for the much reduced grain size of the β-Ti phase in the Grade 7 Ti after annealing.

Discussion

The three primary experimental findings of this study are:

(a) Grain growth of the α-Ti phase in the cold-rolled Grade 4 CP-Ti during annealing at 1000 °C was significantly confined by the Fe-stabilized GB β-Ti phase;

(b) The grain size of the β-Ti phase in the cold-rolled Grade 7 Ti showed a substantial reduction after annealing at 1000 °C; and

(c) Pd generally exists in two different forms in the annealed Grade 7 CP-Ti and both forms of distribution are closely associated with Fe.

Regarding Point (a), the underlying reasons are:

(i). Although Fe has a significant solubility in β-Ti,[1–3] its solubility in α-Ti is trivial.[25] A recent study[8] indicated that the presence of 1280 ppm (0.128 wt.%) of Fe is sufficient to lead to the precipitation of Fe-stabilized β phase at the α-Ti GBs, although this is well below the corresponding ASTM specification (0.2 wt.% Fe).

(ii). Fe is a eutectoid alloying element for Ti [see Fig. 4(b)[26]] and has a negligible solubility in α-Ti at the eutectoid temperature (0.0385 wt.% at 568 °C[26]). Hence, each CP-Ti material is fundamentally a hypereutectoid Ti–Fe alloy. However, the assumed eutectoid reaction ($\beta \rightarrow \alpha + \mathrm{TiFe}$) has rarely been observed even in the eutectoid Ti–Fe

https://doi.org/10.1557/mrc.2014.33 Published online by Cambridge University Press

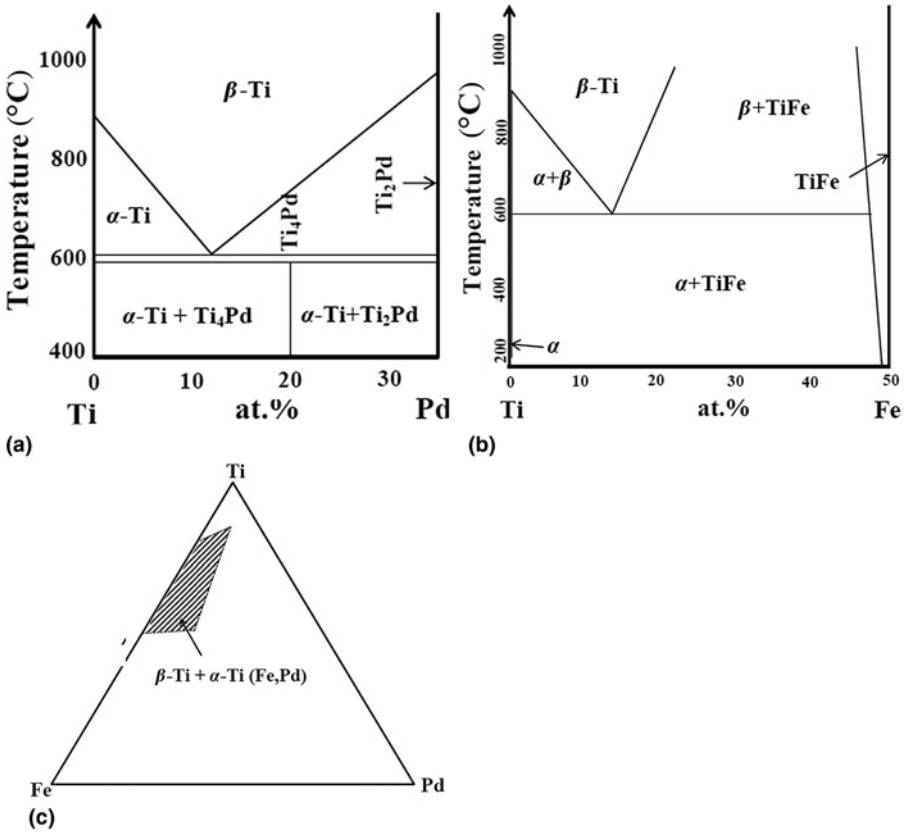


Figure 4. Schematic phase diagrams: (a) Ti–Pd diagram up to 33 at.% Pd, (b) Ti–Fe diagram up to 50 at.% Fe and (c) the isothermal section of the ternary Ti–Fe–Pd phase diagram at 800 °C, showing that there is a region where Fe-stabilized and Pd-containing β-Ti can co-exist with α-Ti containing a small amount of Fe and Pd at 800 °C.

alloy subjected to furnace cooling, due to the sluggish eutectoid reaction rate involved.[27]

These two facts explain why the only other practical way for the extra impurity Fe to exist in the room-temperature microstructure of CP-Ti is to form Fe-stabilized β phases. Assuming the Fe impurity in CP-Ti all participates in the formation of the β phase, it could lead to an estimated volume fraction of ~6% of the β phase based on both the compositional information in β-Ti (~7 at.% Fe as measured by TEM–EDX) and image analysis. According to the particle-pinning model ($R = K \bullet r/f$, where f is the volume fraction of the pinning phase and R is the average radius of grain),[28] the grain size is adversely proportional to the volume fraction of the secondary phase particles. In this regard, having an increased presence of β-Ti phase particles in CP-Ti through adjusting the Fe impurity level is expected to help restrict α-phase growth during the subsequent heat treatment.

Regarding Point (b), the major difference between the Grade 4 CP-Ti and Grade 7 Ti alloy is that the latter contains Pd. As indicated by TEM–EDX, Pd was associated with Fe in the Fe-stabilized β phase [Fig. 3(f)]. It is noticed from the isothermal section of the Ti–Fe–Pd ternary phase diagram at 800 °C, shown in Fig. 4(c)[29] that there is a stage where β-Ti can co-exist with α-Ti. This suggests that reactions like β-Ti (containing higher Fe and Pd) $\rightarrow$ β-Ti (Fe-stabilized) + α-Ti (containing lower Fe and Pd) may have occurred in the Grade 7 Ti alloy during annealing. Such reactions involve redistribution of Pd and Fe away from high temperature β-Ti phases into a mixture of β-Ti and α-Ti phases at lower temperatures. We propose that this solute redistribution enabled the original Fe-stabilized β phases in the cold-rolled Grade 7 Ti alloy to decompose into two phases of finer grain sizes, consistent with the microstructures observed (Figs. 1 and 3). In particular, it is noted that in the absence of Pd, the Fe-stabilized β-Ti phase persisted to room temperature without the expected $\beta \rightarrow \alpha$ transformation at ~882 °C; see Fig. 1 for the results obtained from Grades 1 and 4 CP-Ti samples. This is in contrast to the case of the Grade 7 Ti alloy, further highlighting the key role of Pd in enabling the β-Ti phase refinement through the proposed mechanism.

The last point is about the existing form of Pd in the annealed Grade 7 Ti alloy. We have shown that the presence of Pd is closely associated with Fe in the Grade 7 Ti alloy, existing

https://doi.org/10.1557/mrc.2014.33 Published online by Cambridge University Press

either in the Fe-stabilized β-Ti phase or as a Ti–Fe–Pd intermetallic phase in addition to a small presence in the α-Ti matrix. The specification for the Grade 7 Ti alloy allows a maximum of 0.3 wt.% Fe. This study has thus raised a stimulating question, i.e., what will happen to the distribution of Pd in the Grade 7 Ti alloy if the alloy is made to be essentially Fe-free. This may affect the corrosion resistance of the Grade 7 Ti. Detailed study is needed in that regard.

Conclusions

- When the impurity Fe is adequately present in CP-Ti (e.g., 0.5 wt.% in Grade 4 CP-Ti), the growth of the α-Ti grains can be significantly confined during annealing even at 1000 °C by the pinning effect from the Fe-stabilized, GB β-Ti phases. However, such confinement effects are not observed in Grade 1 CP-Ti which contains a low level of Fe (0.2 wt.%) due to the lack of formation of sufficient Fe-stabilized, GB β-Ti phases.
- The grain size of the Fe-stabilized β-Ti phase in the Grade 7 Ti alloy can be markedly reduced by annealing, from tens of microns (up to ~40 μm) before annealing to 1–2 μm after annealing. Redistribution of Fe and Pd (Pd in particular) from the Fe-stabilized β-Ti phase (containing a high concentration of both Fe and Pd) is responsible for the substantial refinement of the Fe-stabilized β-Ti phase.
- Pd in the as-received (cold-rolled) Grade 7 Ti alloy exists mainly in the Fe-stabilized β-Ti phase. A small percentage of Pd can also be found in an occasionally observed orthorhombic $Ti_{88}Pd_9Fe_3$ phase which is close to the Ti_2Pd_3 intermetallic phase in terms of crystal structure. The distribution of Pd is closely associated with Fe in the Grade 7 Ti alloy.

Acknowledgment

M.Y. acknowledges the support of a JSPS Fellowship (Invitation, Short Term).

References

1. G. Lutjering and J.C. Willams: *Titanium*, 2nd ed. (Springer-Verlag, Berlin, 2007), pp. 185–198.
2. C. Leyens and M. Peters (eds): *Titanium and Titanium Alloys: Fundamentals and Applications* (Wiley-VCH, Weinheim, 2003), pp. 1–35.
3. H. Conrad: Effect of interstitial solutes on the strength and ductility of titanium. *Prog. Mater. Sci.* **26**, 123 (1981).
4. C.S. Brossia and G.A. Cragnolino: Effect of palladium on the corrosion behavior of titanium. *Corros. Sci.* **46**, 1693 (2004).
5. R.W. Schutz: Ruthenium enhanced titanium alloys. *Platinum Met. Rev.* **40**, 54 (1996).
6. A. Biesiekierski, D.H. Ping, Y. Yamabe-Mitarai, and C. Wen: Impact of ruthenium on microstructure and corrosion behavior of β-type Ti–Nb–Ru alloys for biomedical applications. *Mater. Des.* **59**, 303 (2014).
7. M. Yan, S.D. Luo, G.B. Schaffer, and M. Qian: TEM and XRD characterisation of commercially pure α-Ti made by powder metallurgy and casting. *Mater. Lett.* **72**, 64 (2012).
8. M. Yan, S.D. Luo, G.B. Schaffer, and M. Qian: Impurity (Fe, Cl, and P)-induced grain boundary and secondary phases in commercially pure titanium (CP-Ti). *Metall. Mater. Trans. A* **44**, 3961 (2013).
9. M. Yan, M.S. Dargusch, T. Ebel, and M. Qian: A transmission electron microscopy and three-dimensional atom probe study of the oxygen-induced fine microstructural features in as-sintered Ti–6Al–4V and their impacts on ductility. *Acta Mater.* **68**, 196 (2014).
10. http://enterprise.astm.org/filtrexx40.cgi?+REDLINE_PAGES/B863.htm
11. Y. Liu, L.F. Chen, H.P. Tang, C.T. Liu, B. Liu, and B.Y. Huang: Design of powder metallurgy titanium alloys and composites. *Mater. Sci. Eng. A* **418**, 25 (2006).
12. M. Yan, Y. Liu, G.B. Schaffer, and M. Qian: In situ synchrotron radiation to understand the pathways for the scavenging of oxygen in commercially pure Ti and Ti–6Al–4V by yttrium hydride. *Scr. Mater.* **68**, 63 (2013).
13. D.J. Simbi and J.C. Scully: The effect of residual interstitial elements and iron on mechanical properties of commercially pure titanium. *Mater. Lett.* **26**, 35 (1996).
14. R. Zhu, Z. Qin, J.J. Noël, D.W. Shoesmith, and Z. Ding: Analyzing the influence of alloying elements and impurities on the localized reactivity of titanium grade-7 by scanning electrochemical microscopy. *Anal. Chem.* **80**, 1437 (2008).
15. A.V. Polyakov, I.P. Semenova, R.Z. Valiev, Y. Huang, and T.G. Langdon: Influence of annealing on ductility of ultrafine-grained titanium processed by equal-channel angular pressing–conform and drawing. *MRS Commun.* **3**, 249 (2013).
16. D.C. Zhang, J.G. Lin, and C. Wen: Influences of recovery and recrystallization on the superelastic behavior of a β titanium alloy made by suction casting. *J. Mater. Chem. B* **2**, 5972 (2014).
17. R.J. Contieri, M. Zanotello, and R. Caram: Recrystallization and grain growth in highly cold worked CP-Titanium. *Mater. Sci. Eng. A* **527**, 3994 (2010).
18. E.J. Mittemeijer: Recovery, recrystallization and grain growth. In *Fundamentals of Materials Science*, edited by E.J. Mittemeijer (Springer-Verlag, Berlin, Heidelberg, 2010), pp. 463–495.
19. M. Yan, M. Qian, C. Kong, and M.S. Dargusch: Impacts of trace carbon on the microstructure of as-sintered biomedical Ti–15Mo alloy and reassessment of the maximum carbon limit. *Acta Biomater.* **10**, 1014 (2014).
20. P. Krautwas, S. Bhan, and K. Schubert: Structural investigations in systems Ti-Pd and Ti-Pt. *Z. Metallkd.* **59**, 724 (1968).
21. V.N. Eremenko and T.D. Shtepa: Phase diagram of the system titanium-palladium. *Sov. Powder Metall. Met. Ceram.* **11**, 228 (1972).
22. E.M. Sokolovskaya, T.P. Loboda, and U.M. Makanov: Study of interaction of iron and palladium with titanium and zirconium. *Metally* **6**, 166 (1992).
23. J.L. Murray: The Pd-Ti (Palladium-Titanium) system. In *Phase Diagrams of Binary Titanium Alloys*, edited by J.L. Murray (ASM International, Materials Park, OH, 1987), pp. 239–246.
24. M. Yan, Y. Liu, Y.B. Liu, C. Kong, G.B. Schaffer, and M. Qian: Simultaneous gettering of oxygen and chlorine and homogenization of the β phase by rare earth hydride additions to a powder metallurgy Ti–2.25 Mo–1.5 Fe alloy. *Scr. Mater.* **67**, 491 (2012).
25. J. Matyka, F. Faudot, and J. Bigot: Study of iron solubility in alpha-titanium. *Scr. Mater.* **13**, 645 (1979).
26. J.L. Murray: Fe-Ti (Iron-Titanium). In *Phase Diagrams of Binary Iron Alloys*, edited by H. Okamoto (ASM International, Materials Park, OH, 1993), pp. 415–425. [See also H. Okamoto: Fe–Ti (Iron-Titanium). *J. Phase*, 369 (1996)].
27. M. Yan: Microstructural characterisation of as-sintered titanium and titanium alloys. In *Titanium Powder Metallurgy: Science, Technology and Applications*, edited by M. Qian and F.H. Froes (Elsevier and Science Direct, Boston, MA, ISBN: 978-0-800054-0, 2014).
28. N. Moelans, B. Blanpain, and P. Wollants: Pinning effect of second-phase particles on grain growth in polycrystalline films studied by 3-D phase field simulations. *Acta Mater.* **55**, 2173 (2007).
29. H. Okamoto: Fe-Pd (Iron–Palladium). In *Phase Diagrams of Binary Iron Alloys*, edited by H. Okamoto (ASM International, Materials Park, OH, 1993), pp. 319–325.

https://doi.org/10.1557/mrc.2014.33 Published online by Cambridge University Press